HHS Public Access

Author manuscript

*Biomaterials*. Author manuscript; available in PMC 2019 November 01.

Published in final edited form as:

*Biomaterials*. 2018 November ; 183: 54–66. doi:10.1016/j.biomaterials.2018.08.047.

# Nanotopography-Responsive Myotube Alignment and Orientation as a Sensitive Phenotypic Biomarker for Duchenne Muscular Dystrophy

**Bin Xu**[a], **Alessandro Magli**[b,c], **Yoska Anugrah**[e], **Steven J. Koester**[e,d], **Rita C.R. Perlingeiro**[b,c,d], and **Wei Shen**[a,c,d,*]

[a]Department of Biomedical Engineering, University of Minnesota, Minneapolis, Minnesota 55455, USA.

[b]Department of Medicine, University of Minnesota, Minneapolis, Minnesota 55455, USA.

[c]Stem Cell Institute, University of Minnesota, Minneapolis, Minnesota 55455, USA.

[d]Institute for Engineering in Medicine, University of Minnesota, Minneapolis, Minnesota 55455, USA.

[e]Department of Electrical and Computer Engineering, University of Minnesota, Minneapolis, Minnesota 55455, USA.

## Abstract

Duchenne Muscular Dystrophy (DMD) is a fatal genetic disorder currently having no cure. Here we report that culture substrates patterned with nanogrooves and functionalized with Matrigel (or laminin) present an engineered cell microenvironment to allow myotubes derived from non-diseased, less-affected DMD, and severely-affected DMD human induced pluripotent stem cells (hiPSCs) to exhibit prominent differences in alignment and orientation, providing a sensitive phenotypic biomarker to potentially facilitate DMD drug development and early diagnosis. We discovered that myotubes differentiated from myogenic progenitors derived from non-diseased hiPSCs align nearly perpendicular to nanogrooves, a phenomenon not reported previously. We

*Corresponding author. Correspondence and requests for materials should be addressed to Wei Shen (shenx104@umn.edu: Tel: +1 612 624 3771; Fax: +1 612 626 6583). Correspondence for requests of patient-specific materials should be addressed to R.C.R.P. (perli032@umn.edu).

Author contributions

B.X. designed and conducted all the experiments, analyzed the data, and wrote the manuscript; A.M. prepared PSC-derived myogenic progenitors, and characterized DMD hiPSC- derived myogenic progenitors; Y.A. participated in the nanofabrication; K.J.K. supervised nanofabrication; R.C.R.P. oversaw preparation and characterization of PSC-derived myogenic progenitors, and revised the manuscript; W.S. oversaw all aspects of the study, designed all the experiments, analyzed the data, and wrote the manuscript.

Data availability

All data generated and analyzed during the current study are available from the corresponding author upon request.

Competing interests

The authors declare no competing financial interest.

Supplementary data

Supplementary data related to this article are available.

further found that myotubes derived from hiPSCs of a dystrophin-null DMD patient orient randomly, and those from hiPSCs of a patient carrying partially functional dystrophin align approximately 14° off the alignment direction of non-diseased myotubes. Substrates engineered with micron-scale grooves and/or cell adhesion molecules only interacting with integrins all guide parallel myotube alignment to grooves and lose the ability to distinguish different cell types. Disruption of the interaction between the Dystrophin-Associated-Protein- Complex (DAPC) and laminin by heparin or anti-α-dystroglycan antibody IIH6 disenables myotubes to align perpendicular to nanogrooves, suggesting that this phenotype is controlled by the DAPC-mediated cytoskeleton-extracellular matrix linkage.

## Graphical Abstract

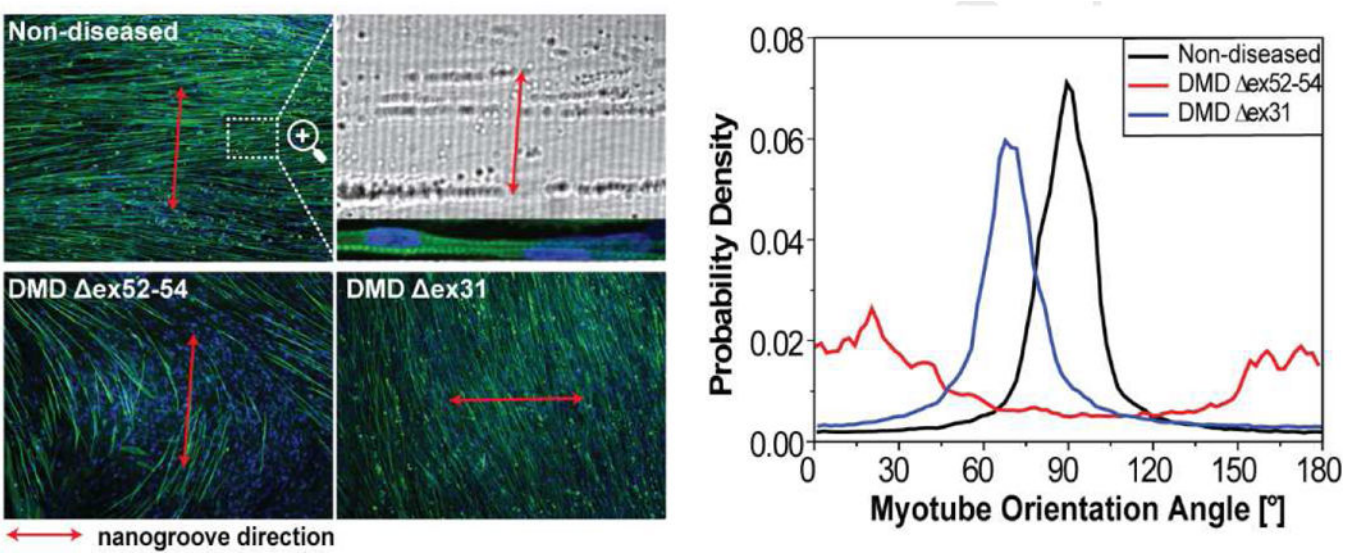


### Keywords

Nanotopography; Duchenne Muscular Dystrophy; stem cells; myotube orientation; Matrigel; laminin

## 1. Introduction

Duchenne Muscular Dystrophy (DMD) is a genetic disorder that causes progressive muscle weakness and wasting, and the patients often die from cardiac and respiratory failure at an age of 20-30s[1]. The disease affects one in 3500 male births worldwide[2]. It is known that DMD is caused by mutations in dystrophin, a cytoplasmic protein essential for muscle function[3, 4]. In healthy skeletal muscle, dystrophin links intracellular cytoskeleton to the extracellular matrix (ECM) through the sarcolemma(muscle cell membrane)-associated Dystrophin- Associated-Protein-Complex (DAPC): the actin-binding domains in dystrophin associate with actin filaments and the C-terminal domain of dystrophin associates with the transmembrane α/β dystroglycan complex, which further binds to laminin in the surrounding basement membrane[5-8]. This cytoskeleton-ECM linkage stabilizes myofibers during muscle contraction and relaxation and is essential for muscle function[4, 5, 9, 10].

When dystrophin is missing or defective, myofibers are less stable and susceptible to chronic injury, causing DMD symptoms and eventually depleting muscle regenerative ability. Given the severe consequences of DMD and its high incidence among genetic disorders, massive efforts have been made to search for DMD treatments[4, 11]. However, there is still no cure for the disease; currently used corticosteroid treatment only slows down disease progression. In addition, despite the advances in genetic testing technologies, there is an average delay of about 2.5 years between onset of DMD symptoms and definitive diagnosis[12, 13], because the dystrophin gene is very large and there are many possible types of pathogenic mutations and some of which require expensive full gene sequencing and even RNA analysis to identify[14]. Typical clinical diagnosis of DMD starts after symptoms become manifest, and genetic testing is conducted only after its necessity is suggested by the results of a series of other examinations such as physical examination, measurement of the serum creatinine phosphokinase level, electromyography, and muscle biopsy[14, 15]. The well-documented negative clinical impact of delayed diagnosis and treatment, together with the ongoing efforts to develop new therapies that potentially can be initiated earlier than corticosteroid treatment, makes early, accurate, and cost-effective diagnosis of DMD increasingly important[12, 13, 16].

The advances in stem cell technologies, particularly those of human pluripotent stem cells (hPSCs), including human embryonic stem cells (hESCs) and human induced pluripotent stem cells (hiPSCs), have provided unprecedented opportunities to engineer human tissues and disease models *in vitro* for screening and validating drugs, facilitating diagnosis, and elucidating pathological mechanisms[17-23]. Human PSCs can be expanded extensively and induced for differentiation towards all somatic cell types, ensuring unlimited sources of healthy and disease- specific human cells, and studies using these cells eliminate the issue of interspecies differences associated with animal models. Patient-derived and disease-specific hiPSCs retain genetic characteristics of donors, and therefore are particularly valuable for studying genetic disorders such as muscular dystrophies. We have previously developed a method to efficiently produce myogenic progenitors from hPSCs by inducible expression of the paired box PAX 7 transcription factor (iPAX7), which are endowed with robust *in vitro* and *in vivo* muscle differentiation potential, representing a valuable tool for disease modeling and regenerative medicine[24].

We hypothesized that engineered cell microenvironments would regulate the behavior of hPSC-derived myogenic progenitors and that the phenotypic disparity between non-diseased and DMD hiPSC-derived myotubes would be enhanced in response to certain microenvironmental cues to yield a DMD biomarker for facilitating drug development and diagnosis. It has been extensively reported that cell phenotypes and functions can be profoundly impacted by biochemical ligands and topographical features engineered on cell culture substrates[25-30]. In particular, micro- and nano-scale anisotropic topographical cues have been extensively used in designing biomimetic microenvironments to engineer skeletal muscle[31-49]. These topographical cues include parallel grooves, waves, wrinkles, and aligned fibers; in most studies, the substrates were functionalized with cell adhesion molecules such as collagen, gelatin, fibronectin, the RGD peptide, laminin, and Matrigel. All these studies reported enhanced myotube alignment along the topographical direction and subsequently improved tissue maturation, highlighting the importance of using anisotropic

topographical cues to advance skeletal muscle tissue engineering. However, the myoblasts used in most of these studies are C2C12 cells (a mouse cell line) and primary murine or human myoblasts. To our knowledge, only one study reported the effects of parallel microgrooves on formation and alignment of hESC-derived myotubes[45], and no study has been reported on using topographical cues to enhance the phenotypic disparity between non-diseased and DMD hiPSC-derived myotubes[32], though it has been reported that parallel nanogrooves could stratify the normal and disease phenotypes of hiPSC-derived cardiomyocytes[50]. Therefore, we examined the behavior of nondiseased and DMD patient-specific myogenic progenitors derived from iPAX7 hPSCs in response to topographically patterned parallel grooves and substrate-bound cell adhesion molecules during myogenic differentiation.

## 2. Results and Discussion

### 2.1. Myotubes differentiated from hESC-derived myogenic progenitors align nearly perpendicular to topographical nanogrooves patterned on Matrigel-functionalized substrates.

We set out to examine the behavior of hESC-derived myogenic progenitors undergoing myogenic differentiation on polydimethylsiloxane (PDMS) substrates patterned with parallel nanogrooves (800 nm groove/ridge widths and 400 nm depth; Supplementary Fig. 1) and functionalized with Matrigel. This topographical feature was chosen because muscle cells are anatomically aligned in native tissue and parallel nanogrooves were expected to promote myotube alignment. Matrigel (reconstituted basement membrane extracted from Engelbreth-Holm-Swarm (EHS) mouse sarcoma) was chosen because the basement membrane is the ECM immediately adjacent to muscle cells in native tissue[6, 51]. Myogenic progenitors were prepared from iPAX7 hESC by inducing PAX7 expression with doxycycline(dox) as previously reported[24], seeded on the substrates at a density of $2.5\times10^5$ cells/$cm^2$, cultured in a dox- containing expansion medium for one day, and subsequently induced for differentiation in a dox- free myogenic differentiation medium (medium components are listed in Supplementary Information). Noticeable cell elongation was observed on day 3 upon differentiation induction, and formation of long, multinucleated myotubes was obvious after 2 weeks. Immunofluorescent staining of the myotubes for sarcomeric α-actinin revealed that they possessed sarcomeres giving the striated appearance and aligned in a consistent direction throughout the entire area of each substrate (Fig. 1a). We then used bright-field optical microscopy to determine the nanogroove direction on each substrate. Remarkably, we found all the myotubes aligned nearly perpendicular to nanogrooves (Fig. 1b). In contrast, myotubes differentiated from the same cells on flat, Matrigel-functionalized control substrates oriented randomly (Fig. 1c).

We further quantitatively determined myotube orientation distribution using the Directionality plugin in ImageJ/Fiji[52, 53]. The orientation angle is defined as 90° when a myotube aligns perpendicular to grooves and as 0°/180° when a myotube aligns parallel to grooves. An arbitrary direction is used as the 0° reference for samples cultured on flat controls. Fluorescent images acquired at a low magnification (with a 5x objective) were analyzed. The probability density function (p.d.f.) of myotube orientations has a single,

narrow, and high peak near 90° for samples cultured on nanogrooved substrates (Fig. 1d), confirming that the myotubes aligned nearly perpendicular to nanogrooves throughout each entire substrate. Each p.d.f. curve was fitted to a Gaussian function (equation (1)), and the resulting peak position (mean myotube orientation angle) is highly reproducible for myogenic progenitors prepared in different batches. Analysis of 9 p.d.f. curves revealed a myotube orientation angle of 86.4°±2.1° (mean±S.D.). In contrast, the orientation p.d.f. of myotubes cultured on the flat control does not have a narrow and high peak near 90° (Fig. 1d). Instead, low values of probability density spread throughout the whole angle range (Fig. 1d), suggesting random orientations of these myotubes (the wide and low peak in the curve may result from the tendency of myotubes to align locally according to the directional instruction provided by initially formed myotubes during myogenesis[54]). We further examined samples cultured for 4 weeks, and the myotubes showed the same alignment and orientation as those cultured for 2 weeks (Supplementary Fig. 2). To our knowledge, this is the first study reporting differentiating myotubes aligning perpendicular to topographically patterned grooves consistently throughout the whole area of a culture.

### 2.2. Myotubes align perpendicular only to submicron grooves.

We then examined whether the groove feature size would affect myotube alignment and orientation. Human ESC-derived myogenic progenitors were cultured on Matrigel-functionalized PDMS substrates patterned with 500-nm, 1000-nm, 1500-nm, or 3000-nm wide grooves (Supplementary Fig. 1) and induced to undergo myogenic differentiation for 2 weeks. The myotubes aligned in a consistent direction in each sample, but the orientation of aligned myotubes relative to grooves varied significantly with the feature size. The myotubes cultured on 500-nm or 1000-nm grooved substrates aligned nearly perpendicular to the grooves, similar to those on 800-nm grooved substrates. In contrast, the myotubes cultured on 1500-nm or 3000-nm grooved substrates aligned nearly parallel to the grooves (Fig. 2a). For all the samples, the p.d.f. of myotube orientations has a single, narrow, and high peak. The peak is near 90° when the groove feature size is 500 nm or 1000 nm and near 0°/180° when the feature size is 1500 nm or 3000 nm (Fig. 2b). The myotube orientation angle (mean±S.D.) is 86.2°±2.4°, 83.8°±4.8°, 13.0°±10.1°, and 3.6°±2.8° (n=9) when the feature size is 500 nm, 1000 nm, 1500 nm, and 3000 nm, respectively (Fig. 2c). These results suggest that myotubes differentiated from hESC-derived myogenic progenitors align in a highly consistent direction on each Matrigel-functionalized, grooved substrate, but perpendicular alignment relative to grooves only occurs when the feature size is on the submicron scale.

### 2.3. Matrigel or laminin functionalization on substrates is key to enabling perpendicular myotube alignment to nanogrooves.

We further examined whether myotube alignment and orientation on nanogrooved substrates would be affected by cell adhesion molecules functionalized on the substrates. Human ESC-derived myogenic progenitors were cultured on 800-nm grooved substrates functionalized with gelatin, the RGD peptide, fibronectin, and type I collagen, respectively. Myotubes aligned in a consistent direction on each substrate, but interestingly, they all aligned nearly parallel to nanogrooves (Fig. 3a), in contrast to perpendicular myotube alignment on Matrigel- functionalized substrates having the same topographical pattern. The p.d.f. of

myotube orientations has a single, narrow, and high peak near 0°/180° for all these samples (Fig. 3b), in contrast to a peak near 90° for the samples cultured on Matrigel-functionalized substrates (Fig. 1d). These results suggest that cell adhesion molecules functionalized on nanogrooved substrates profoundly affect the orientation of aligned myotubes. Matrigel, which is reconstituted basement membrane containing major components of the ECM immediately adjacent to muscle cells in native tissue, plays an essential role in enabling myotubes to align perpendicular to nanogrooves.

To find out which component in Matrigel is essential for this newly discovered phenotype, we examined the alignment and orientation of myotubes differentiated from hESC- derived myogenic progenitors on 800-nm grooved substrates functionalized with EHS mouse laminin-111 or type IV collagen, two major components in Matrigel. Perpendicular myotube alignment was observed on laminin-functionalized substrates, with the myotube orientation p.d.f. having a single, narrow, and high peak near 90°; parallel myotube alignment was observed on collagen-IV-functionalized substrates, with the myotube orientation p.d.f. having a single, narrow, and high peak near 0°/180° (Fig. 3). We further examined the alignment and orientation of hESC-derived myotubes on 800-nm grooved substrates functionalized with human laminin- 111 and human laminin-211, and observed that the myotubes aligned perpendicular to the nanogrooves, with the myotube orientation p.d.f. having a single, narrow, and high peak near 90° (Fig. 3). Therefore, all the tested laminins permit perpendicular myotube alignment regardless of their origins and types, probably because different laminin types share similar binding sites for a- dystroglycan on the surface of muscle cells[7, 55, 56]. It is known that laminin is structurally and functionally important in native muscle tissue: it interacts with the DAPC through the transmembrane α/β dystroglycan complex and disruption of this interaction impairs muscle function[5-8]. The observation that laminin also plays an indispensable role in enabling perpendicular myotube alignment relative to nanogrooves suggests that this phenotype may have a correlation with muscle function.

### 2.4. Myotubes differentiated from other myogenic cells can also align perpendicular to nanogrooves.

To find out whether perpendicular myotube alignment relative to nanogrooves on Matrigel-functionalized substrates is unique to hESC-derived myogenic progenitors, we examined myotubes differentiated from a variety of other non-diseased myogenic cells, including hiPSC-derived myogenic progenitors, primary human skeletal myoblasts isolated from adult donors, iPAX3 mouse ESC(mESC)-derived myogenic progenitors[57], and C2C12 cells (immortalized skeletal myoblasts derived from adult mice[58]). The myotubes differentiated from hiPSC-derived myogenic progenitors exhibited the same behavior as those from hESC-derived myogenic progenitors: they aligned nearly perpendicular to grooves when the feature size was 500 nm or 800 nm, but aligned nearly parallel to grooves when the feature size was 1500 nm or 3000 nm (Fig. 4 and Supplementary Fig. 3). The myotubes differentiated from primary human skeletal myoblasts, mESC-derived myogenic progenitors, and C2C12 cells aligned nearly perpendicular to grooves when the feature size was 500 nm (Fig. 4), and aligned nearly parallel to grooves when the feature size was 800 nm, 1500 nm, or 3000 nm (Supplementary Fig. 4). Therefore, all examined myotubes, regardless whether

they have a human or murine origin and whether they are PSC-derived or adult myoblasts, aligned nearly perpendicular to topographical grooves when the feature size was sufficiently small, though the feature size at which the myotube orientation transitioned from perpendicular to parallel was different. We further examined two types of non-muscle cells, human umbilical vein endothelial cells (HUVECs) and 3T3 fibroblasts, cultured on the same substrates. Cell elongation in the direction perpendicular to grooves was not observed regardless of the feature size (Supplementary Fig. 5). Therefore, perpendicular alignment to nanogrooves on Matrigel- functionalized substrates appears to be a universal property for myotubes differentiated from non-diseased myogenic cells, but not a universal property for other cells.

Using anisotropic topographical cues to enhance myotube alignment and maturation has been investigated previously, and all the studies reported nearly parallel myotube alignment relative to the topographical direction regardless of the feature size[33, 35-37, 39-43, 45]. In particular, the Kim laboratory reported that primary mouse muscle cells cultured on biodegradable poly(lactic-co-glycolic acid) patches patterned with a nanotopography similar to what we used (800 nm groove/ridge widths and 600 nm depth) and coated with gelatin differentiated into myotubes having enhanced alignment along the nanogroove direction and maturity[36, 40]. These studies highlight the importance of anisotropic nanotopographies in skeletal muscle tissue engineering for regenerative medicine and tissue modeling. On the other hand, the novelty of our study is the new discovery that non-diseased myotubes align perpendicular to nanogrooves when the substrates are functionalized with Matrigel or laminin. Lack of laminin on nanogrooved substrates most likely accounts for the parallel rather than perpendicular myotube alignment observed in these two studies even though a nanotopography similar to ours was used. These results are in fact consistent with our results, as we observed nearly parallel myotube alignment on substrates functionalized with gelatin, the RGD peptide, fibronectin, type I collagen, or type IV collagen. Therefore, both the previous reports and the present study suggest that perpendicular myotube alignment relative to nanogrooves requires an engineered cell microenvironment mimicking that of native muscle tissue, in which laminin is present to interact with the DAPC.

### 2.5. Myotube alignment and orientation on nanogrooved, Matrigel-functionalized substrates can precisely distinguish hiPSCs derived from a non-diseased individual, a dystrophin-null DMD patient, and a DMD patient carrying partially functional dystrophin.

Next, we investigated whether the ability of myotubes to align perpendicular to nanogrooves would be impaired for cells derived from patients carrying genetic mutations for DMD. To address this question, myogenic progenitors derived from hiPSCs of two DMD patients, one exhibiting symptoms early and clinically diagnosed at age 2 with a deletion of exons 52-54 in the dystrophin gene (Δex52-54) that completely nullifies dystrophin and the other exhibiting symptoms at a later age and clinically diagnosed at age 7 with a deletion of exon 31 (Δex31) that allows partially functional dystrophin to be produced, were examined side-by-side with a non-diseased hiPSC-derived myogenic progenitor control. The investigator conducting the experiments and data analysis was blinded to the experimental groups. The cells were induced to undergo myogenic differentiation on Matrigel-functionalized substrates patterned with 500-nm or 800-nm wide grooves for 2 weeks. The myotubes

differentiated from these three types of cells exhibited strikingly different alignment and orientation, allowing the investigator to accurately determine the identity of each myogenic progenitor sample (Fig. 5a). The myotubes differentiated from one myogenic progenitor sample aligned nearly perpendicular to nanogrooves throughout the entire culture area, and this particular sample was inferred to be non-diseased. The myotubes differentiated from the second myogenic progenitor sample appeared to orient randomly, and it was inferred to be derived from the dystrophin-null DMD patient carrying the Δex52-54 mutation. The myotubes differentiated from the third myogenic progenitor sample aligned in a consistent direction throughout the entire culture area, but the angle between the myotube and nanogroove directions obviously deviated from 90°. This third sample was inferred to be myogenic progenitors derived from the DMD less affected patient carrying the Δex31 mutation. The identity of each hiPSC-derived myogenic progenitor sample was confirmed by the collaborator providing these samples.

For both non-diseased and DMD less affected (carrying partially functional dystrophin) cells, the p.d.f. of myotube orientations has a single, narrow, and high peak, suggesting that these myotubes aligned in a consistent direction; the peak is near 90° for the former and near 70° for the latter (Fig. 5b). In contrast, the p.d.f. of myotube orientations for the dystrophin-null DMD cells does not have a narrow and high peak (Fig. 5b). Instead, low values of probability density spread throughout the whole angle range with some wide, low peaks, suggesting that these myotubes did not have a consistent alignment direction. The differences between the p.d.f. curves are so striking that the three cell types can be distinguished readily with high accuracy. Quantitative analysis revealed the following myotube orientation angles (mean±S.D.) for non- diseased and DMD less affected cells: 84.6±3.1° and 84.1±3.2° for the former and 71.3±5.6 ° and 69.0±7.1° for the latter when the feature size is 500 nm and 800 nm, respectively (Fig. 5c). Even though DMD less affected myotubes align in a highly consistent direction, the mean orientation angle is approximately 14° lower than that of non-diseased myotubes. Such substantial deviation makes this phenotype a sensitive biomarker to identify even DMD less affected cells.

To further confirm the reliability of the method to detect DMD cells, myogenic progenitors derived from a different hiPSC clone from each of these two DMD patients were prepared, and the investigator blinded to the cell groups repeated the experiments on 800-nm grooved substrates. The myotubes differentiated from one cell sample aligned in a consistent direction and quantitative analysis revealed an alignment angle of 75.4 ± 1.0°; the myotubes differentiated from the other cell sample oriented randomly (Supplementary Fig. 6). The collaborator providing the cell samples confirmed that the former is from the DMD patient carrying the Δex31 mutation and the latter is from the DMD patient carrying the Δex52-54 mutation.

When cultured on Matrigel-functionalized substrates patterned with 3000-nm wide grooves, the myotubes differentiated from both types of DMD myogenic progenitors aligned nearly parallel to grooves (Supplementary Fig. 7), similar to those differentiated from non-diseased cells (Supplementary Fig. 3). Therefore, only the substrates patterned with submicron grooves, which allow nearly perpendicular alignment for non-diseased myotubes, can

distinguish the cells derived from non-diseased individuals and DMD patients affected by different mutations.

Myotubes derived from the non-diseased individual, dystrophin-null DMD patient, and DMD less affected patient exhibited substantially enhanced disparities in their alignment and orientation on nanogrooved, Matrigel-functionalized substrates, which may potentially serve as a DMD biomarker. A previous study pioneered the use of nanogrooved substrates to stratify the normal and disease phenotypes of hiPSC-derived cardiomyocytes (hiPSC-CMs) [50]. The topography was similar to what we used (800 nm groove/ridge widths and 600 nm depth) and the patterned substrates were coated with fibronectin. The distribution of actin fiber angles showed a peak near 0° for all examined hiPSC-CMs (the parallel rather than perpendicular alignment may arise from lack of laminin on nanogrooved substrates and/or different muscle cell type), though the peak for normal hiPSC-CMs was narrower and higher than that for dystrophin-null DMD hiPSC-CMs. In our study, we observed considerable batch-to-batch variations in the peak width and height of p.d.f. curves for cells derived from the same individual and the same clone. Therefore, it might not be highly accurate to distinguish non-diseased and DMD cells on the basis of peak width and height of p.d.f. curves when all the cells align parallel to nanogrooves. In contrast, our method distinguishes non-diseased and DMD cells on the basis of the highly reproducible peak position (mean orientation angle) in each p.d.f. curve. This high reproducibility, in combination with prominent deviations of disease phenotypes from the nondiseased phenotype, makes the method reported here highly sensitive and accurate. In addition, our method is capable of distinguishing diseased cells having partially functional dystrophin from both non-diseased and dystrophin-null cells. Disease models having such capability have never been reported.

A variety of approaches have been used to create skeletal muscle models *in vitro* for disease modeling and drug discovery, with an emphasis on engineering biomimetic cell microenvironments to promote muscle maturation to mimic muscle physiology and to recapitulate disease phenotypes[32, 59]. Anisotropic topographical cues have been proven to powerfully enhance myotube alignment and subsequently tissue maturation[33, 35, 36, 39]. Tissue models derived from hESCs and hiPSCs represent a powerful tool in drug discovery and development, because they address the issue of interspecies differences associated with animal models and offer the opportunity to detect patient-specific drug responses. However, little has been reported on the effects of anisotropic topographical cues on hPSC-derived skeletal muscle[45], though the importance of anisotropic topographical cues in promoting alignment and subsequently structural and functional maturation of hPSC-derived cardiomyocyte has been more extensively reported[17, 50, 60-66]. Carson et al. investigated hiPSC-CMs cultured on substrates patterned with 350- to 2000-nm parallel grooves and functionalized with RGD[60]. All feature sizes promoted hiPSC-CM alignment along the groove direction, and the peak effects on enhancing cell alignment and subsequent maturation were observed on 800-nm grooved substrates, where the majority of the cells fell within 5° of the groove direction. This substrate was used to stratify the normal and disease phenotypes of hiPSC-CMs on the basis of actin fiber distribution, cell elongation, and contraction velocity anisotropic ratio[50]. Several studies reported using anisotropic topographical cues to improve the sensitivity of hPSC-CM tissue models to drugs[63, 64, 66]. Human iPSC-CMs cultured on flexible nanofilms coated with aligned piezoelectric

microfibers showed higher expression of cardiomyocyte markers, higher cellular alignment along the microfibers, higher metabolic maturation, and higher contractility than those cultured on a flat control, and the aligned and more mature hiPSC-CMs exhibited higher sensitivity to cardiotoxic compounds and cardiomyocyte contraction modulators[66]. Human ESC-derived ventricular cardiomyocytes cultured on substrates having parallel wrinkles showed improved alignment along the topographical direction, sarcomeric structure, and calcium cycling properties; the aligned tissue model exhibited anisotropic electrical conduction like native human ventricle and showed reduced spontaneous arrhythmias to provide a physiological baseline, and this model successfully detected cardiotoxicity of several drugs that previously failed in clinical trials or were withdrawn from the market[63, 64]. These studies highlight the utility of anisotropic topographical cues to improve the efficacy of hPSC-CM tissue models in drug screening and disease modeling. Our study is the first to use anisotropic topographical cues to enhance phenotypic disparity between non-diseased and DMD hiPSC-derived skeletal muscle cells. In addition, our study is the first to offer a model capable of distinguishing DMD cells having partially functional dystrophin from both non-diseased and dystrophin-null DMD cells.

### 2.6. Disruption of the DAPC-laminin interaction disenables myotubes to align perpendicular to nanogrooves.

Our results showed that both intact dystrophin in cells and the presence of Matrigel or laminin on substrates are required for perpendicular myotube alignment, suggesting that the phenotype is controlled by the DAPC-mediated cytoskeleton-ECM linkage. To further confirm the important role of this linkage, we added heparin or anti-α-dystroglycan antibody IIH6 to the culture media to disrupt the DAPC-laminin interaction when hESC-derived myogenic progenitors were cultured on Matrigel-functionalized, 800-nm grooved substrates. Both heparin and IIH6 have been previously used to inhibit the DAPC-laminin interaction in skeletal muscle; heparin disrupts the interaction through its binding to laminin, and IIH6 blocks the interaction through its binding to a-dystroglycan, which is an essential DAPC component interacting with laminin in native muscle[67, 68]. In the presence of 1 mg/ml heparin, myotubes aligned parallel to the nanogrooves and the p.d.f. of myotube orientations shows a high peak near 0°/180°. In the presence of 70 μg/ml IIH6, the p.d.f. of myotube orientations shows a wide and low peak at approximately 40° (Fig. 6). In both experiments, the myotube orientations deviated significantly from the perpendicular direction relative to the nanogrooves, suggesting that disruption of the DAPC-laminin interaction disenables perpendicular myotube alignment. These results confirmed the essential role of the DAPC-mediated cytoskeleton-ECM linkage in regulating perpendicular myotube alignment relative to nanogrooves.

### 2.7. Possible roles of the DAPC and focal adhesions in mediating topography-responsive myotube orientation.

Cell alignment and orientation in response to anisotropic topographical cues has been extensively examined for various cell types, including muscle cells. Typically cells elongate in the direction parallel to grooves or aligned fibers[29, 31-50, 60-66, 69], and only a few exceptions have been reported. Human corneal epithelial cells transition from parallel to perpendicular orientation relative to grooves as the feature size decreases from microscale to

nanoscale when cultured in Epilife medium[70]. Neurites growing from certain embryonic neurons orient perpendicular to shallow, narrow grooves and parallel to deep, wide ones[71, 72]. Fetal myoblasts align parallel to the direction of deep microgrooves, but approximately 25% of these myoblasts align perpendicular to the direction of shallow microgrooves[73]. C2C12 cells cultured on dual-level topographical matrices combining parallel nanofibers and a microgrooved topography formed myotubes aligning at an angle of 24° relative to the fiber orientation, while those cultured on scaffolds having only nanofibers aligned parallel to the fibers[74]. The detailed mechanisms underlying how cells sense anisotropic topographical stimuli and transduce them to cell orientation, either parallel orientation in the majority of studies or deviation from parallel orientation and perpendicular orientation in the rare cases, remain not fully elucidated. However, it has been well recognized that the cytoskeleton-ECM linkage mediated by focal adhesion protein complexes (FAs), which contain transmembrane integrin receptors, plays a critical role in determining topography-responsive orientation for non-muscle cells[75-78].

The DAPC and FAs are both essential sarcolemma-associated protein complexes connecting cytoskeleton to the ECM in muscle[9], and our results suggest that they both play roles in regulating topography-responsive myotube orientation. We observed that non-diseased myotubes align perpendicular to nanogrooves only when laminin is present on substrates and that DMD myotubes having mutated dystrophin do not exhibit this phenotype even on laminin- functionalized substrates. Furthermore, when we blocked the DAPC-laminin interaction, myotubes failed to align perpendicular to nanogrooves. These results clearly suggest that perpendicular myotube alignment is controlled by the DAPC-mediated cytoskeleton-ECM linkage. On the other hand, nanogrooved substrates functionalized with adhesion molecules only interacting with integrins (gelatin, the RGD peptide, fibronectin, and collagen) guide myotubes to align parallel to nanogrooves, suggesting that the parallel orientation is mediated by integrin- containing FAs.

Since myotube orientation always aligns with the direction of myofibrils[79], the DAPC and FAs most likely mediate topography-responsive myotube orientation through their regulation on myofibrillogenesis. Although many details of myofibrillogenesis remain unclear, it has been widely reported that FAs are an important regulator in the initial stage of myofibrillogenesis, and a few studies suggest that other transmembrane protein complexes could also play a role[80-84]. A hypothetical model that could explain the observed influences of the groove feature size, the substrate-bound cell adhesion molecules, and dystrophin mutations on myotube orientation is illustrated in Supplementary Fig. 8. It is likely that FAs play an early role, and the polarized FA arrangement along both micro- and nano-scale grooves guides myofibrils to orient parallel to grooves if FA maturation is not hindered by geometric constraints and/or if the DAPC-mediated cytoskeleton-ECM linkage is absent[75-77]. The DAPC may play a later role and possibly determine myofibril orientation only if FA maturation is hindered by submicron grooves. On microgrooved substrates, FA maturation is not restricted and FAs drive myofibrils to align parallel to the microgrooves regardless of whether laminin is present or whether cells have mutated dystrophin. On nanogrooved substrates, FAs are restricted mainly on ridges, as reported by previous studies[30, 85-87] and supported by our own data (Fig. 7). Such restriction hinders FA maturation[88-90], rendering the control of myofibril orientation to the DAPC-mediated

cytoskeleton-ECM linkage, though the reason why the later regulator sets the orientation perpendicular to nanogrooves is unclear. On nanogrooved substrates having no laminin, even though FA maturation is hindered, the FAs along the ridge/groove direction guide myofibrils to orient parallel to the nanogrooves because the later regulator is absent.

### 2.8. Potential applications of nanotopography-responsive myotube orientation on Matrigel (or laminin)-functionalized substrates as a DMD biomarker.

We showed that nanogrooved, Matrigel (or laminin)-functionalized substrates allow myotubes derived from non-diseased, less-affected DMD, and severely-affected DMD hiPSCs to exhibit prominent differences in alignment and orientation, making these cells precisely distinguishable. On the molecular level, we showed the importance of the DAPC-mediated cytoskeleton-ECM linkage in enabling these phenotypes. It is well-known that the DAPC- mediated cytoskeleton-ECM linkage is essential for muscle function, and defective DAPC or defective DAPC-laminin interaction due to mutations in dystrophin and other involving components underlies the pathology of many muscular dystrophies[4, 9, 10, 91-95]. The importance of the DAPC-mediated cytoskeleton-ECM linkage in regulating both nanotopography-responsive myotube orientation and muscle function underlies the observed correlation between the *in vitro* disease phenotypes and clinically diagnosed DMD patients affected by different dystrophin mutations, providing the basis for establishing aberrant myotube alignment and orientation on these engineered substrates as a potential DMD biomarker.

One potential application of this biomarker is to serve as a simple and cost-effective phenotypic readout to detect drug effects in high throughput screening (HTS) for DMD drugs. The HTS-based drug discovery has been recognized as a powerful approach[96, 97]. The hiPSC- derived myogenic progenitors provide an unprecedented opportunity to create patient-specific human DMD models to screen drugs based on phenotypic readouts, which address the limitations of molecular-target-based readouts in missing off-target and polypharmacological effects of a drug[98, 99]. Since cost-effectiveness and ease of operation are important criteria for translational applications such as HTS-based drug discovery, we further examined whether data analysis could be conducted using bright-field images. The results yielded from bright-field and fluorescent images of the same frame are highly consistent for all tested conditions (Fig. 8), suggesting that immunofluorescent staining, which is costly and time-consuming, is unnecessary to evaluate myotube alignment and orientation as a DMD biomarker. Therefore, this phenotypic readout can be readily adapted for high-throughput formats to search for effective drugs capable of switching DMD hiPSC-derived myogenic progenitors to non-diseased or less-affected phenotypes.

Another potential application of this biomarker is to facilitate early diagnosis and screening for DMD (and possibly for congenital muscular dystrophies caused by defective a-dystroglycan as well[100]). Despite the advances in genetic testing technologies, the well-documented diagnostic delay and the negative impact of consequently delayed treatment makes early DMD diagnosis increasingly important[12, 13, 16]. Assessing the alignment and orientation of hiPSC-derived myotubes on nanogrooved, Matrigel (or laminin)-

functionalized substrates can potentially serve as a complementary tool to facilitate early identification of DMD.

## 3. Conclusions

We discovered that myotubes differentiated from non-diseased hPSC-derived myogenic progenitors align nearly perpendicular to nanogrooves and those differentiated from DMD hiPSC-derived myogenic progenitors exhibit prominent deviations from perpendicular alignment when these cells are cultured on nanogrooved, Matrigel (or laminin)-functionalized substrates, verifying our hypothesis that the phenotypic disparity between non-diseased and DMD cells could be enhanced by combined topographical and biochemical cues carefully engineered in the cell microenvironment. The differences in myotube alignment and orientation between the cells derived from a non-diseased individual, a dystrophin-null DMD patient, and a DMD patient carrying partially functional dystrophin are so striking that each cell type can be accurately identified by investigators blinded to the experimental groups. Substrates engineered with micron-scale grooves and/or cell adhesion molecules only interacting with integrins guide all myotubes to align parallel to the grooves and lose the ability to distinguish different cell types. On the molecular level, we showed the important role of the DAPC-mediated cytoskeleton-ECM linkage in regulating perpendicular myotube alignment, as we observed that both intact dystrophin in cells and the presence of laminin on substrates are required for this phenotype, and disruption of the DAPC-laminin interaction disenables perpendicular myotube alignment. Myotube alignment and orientation on nanogrooved, Matrigel (or laminin)-functionalized substrates may serve as a sensitive and accurate phenotypic DMD biomarker to potentially facilitate DMD drug development and early diagnosis.

## 4. Methods

### 4.1. Fabrication of pattern templates and cell culture substrates.

A layer of 520-nm thick silicon oxide was deposited on a Czochralski silicon wafer (4 inches in diameter; Silicon Quest International) through plasma enhanced chemical vapor deposition (PECVD) (Surface Technology Systems) at a rate of 372 Å per minute. The wafer was heated on a hot plate at 110 °C for 5 minutes to remove moisture, immediately followed by treatment in hexamethyldisilazane (Sigma-Aldrich) vapor for one minute to promote photoresist adhesion. Photoresist S1813 (Microchem) was spin-coated on the wafer at a speed of 4000 rpm for 30 seconds to obtain a 1.4 μm-thick coating, followed by a soft bake at 110 °C for 5 minutes. The wafer and a chrome mask were loaded into a Canon 2500 i3 stepper (Canon) and exposed to ultraviolet light with a dose of 95 $mJ/cm^2$ and a focus offset of −0.2 μm to photolithographically create desired patterns. The wafer was developed in an MF319 developer (Microchem) for 45 seconds, hard baked at 120°C for 3 minutes, cleaned by oxygen plasma for 45 seconds (Surface Technology Systems), and permanently etched by nitride at a rate of 370 Å per minute (the time was controlled to yield a 400-nm etching depth). The remaining photoresist was thoroughly removed with acetone. Templates patterned with 500-nm, 800-nm, 1000-nm, 1500-nm and 3000-nm wide parallel grooves (groove and ridge widths are the same) were fabricated. The groove depth was 400 nm for

all the patterns. To allow patterns to be readily transferred to PDMS surfaces, the wafer was treated with chlorotrimethylsilane (Sigma-Aldrich) for 1 minutes and washed with acetone.

To fabricate PDMS films, the Sylgard 184 PDMS precursor and curing agent were mixed at a 10:1 mass ratio, cast on a patterned wafer, vacuumed for 1 hour at room temperature to remove trapped air, and cured at 37 °C overnight. Each PDMS film (2 mm thick) was carefully peeled off the wafer and further cured at 120 °C in a vacuum oven for one week. For surface modification, each film was sonicated in 70% (v/v) ethanol for 30 minutes, cleaned with oxygen plasma (PDC-32G, Harrick Plasma), and allowed to react with a solution of 3- glycidoxypropyltrimethoxysilane (Acros Organics; 10% (v/v) solution prepared in 180 proof ethanol; pH 4.5) at room temperature overnight. After washing with ethanol and PBS, the film was cut into 1 cm x1 cm squares, placed in a 24-well plate, and further modified with a biopolymer solution (prepared in PBS; pH 7.8) at 4 °C for 48 hours. The biopolymer solutions used in the study include growth factor reduced Matrigel (BD Biosciences), gelatin (Sigma- Aldrich), human fibronectin (BD Bioscience), rat tail type I collagen (BD Bioscience), cysARGD[101], human type IV collagen (Sigma-Aldrich), laminin-111 produced by Engelbreth- Holm-Swarm mouse sarcoma cells (Sigma-Aldrich), and recombinant human laminin-111 and laminin-211 (BioLamina) (0.1% (w/v) for gelatin, 400 μM for cysARGD, and 0.1 mg/ml for the other biopolymer solutions). Each modified PDMS film was washed with cold PBS twice, and the empty space surrounding the film in the well was filled with agarose hydrogel (1.5% w/v, Invitrogen). Each well was further washed 3 times with Dulbecco's modified Eagle's essential medium (DMEM, Invitrogen) containing 1% Penicillin and Streptomycin, followed by sterilization under 254 nm ultraviolet light for 1 hour in a biological safety cabinet.

### 4.2. Cell culture.

Myogenic progenitors derived from hESCs, hiPSCs, and mESCs were generated through inducible expression of the paired box transcription factor PAX7 (for hESCs and hiPSCs) [24] or PAX3 (for mESCs)[57] as previously described. Characterization of DMD hiPSC-derived myogenic progenitors carrying the Δex52-54 mutation (DMD1705) was reported in a previous study[102]; characterization of DMD hiPSC-derived myogenic progenitors carrying the Δex31 mutation is presented in the Supplementary Information of the present study (Supplementary Fig. 9). For subculture, hPSC-derived myogenic progenitors were seeded at a density of $2\times 10^4$ cells/cm$^2$ and cultured in a dox-containing expansion medium until 100% confluence was reached. Murine myogenic cells (mESC-derived myogenic progenitors and C2C12 cells) and primary human skeletal myoblasts (Thermofisher) were subcultured in their respective expansion media similarly except that 70% confluence was reached in each passage. Medium was changed every two days. For experiments, myogenic cells (passage 3 to 4 for PSC-derived myogenic progenitors, passage 5 for primary human skeletal myoblasts, and passage 13 to 16 for C2C12 cells) were seeded on patterned PDMS substrates at a density of $2.5\times10^5$ cells/cm$^2$ and cultured in their respective expansion media for one day, followed by switching the media to their respective differentiation media. During differentiation, half medium was changed every two days. The samples were examined after 2 or 4 weeks of culture in differentiation media. Human umbilical vein endothelial cells (from Lonza, passage 5) and 3T3 fibroblasts were cultured on patterned

substrates similarly in their respective growth media. The composition of each medium is listed in Table SI in Supplementary Information.

To inhibit the interaction between the DAPC and laminin and evaluate its effect on the orientation of hESC-drived myotubes on Matrigel-functionalized, 800-nm grooved substrates, 1 mg/ml heparin sodium salt (Sigma-Aldrich) or 70 μg/ml anti-α-dystroglycan antibody IIH6 (Developmental Studies Hybridoma Bank, University of Iowa) was added in cell culture media, and the cells were cultured in the same manner as described above.

### 4.3. Immunocytochemistry.

Muscle cells were fixed with 4% paraformaldehyde, permeabilized with 0.5% Triton X- 100, blocked with 5% bovine serum albumin, and stained with an anti-sarcomeric α-actinin antibody (Sigma-Aldrich; 1:300 dilution) for sarcomere structures or anti-paxillin antibody (Biolegend, 1:100 dilution) for FAs, followed by staining with goat anti-mouse AlexaFluor488 (1:500 dilution) and the Hoechst 33342 nuclear marker (10 μg/ml).

### 4.4. Image acquisition.

To observe muscle alignment and striation, cells were imaged on a Zeiss Axio Observer inverted microscope equipped with ApoTome. For striation, fluorescent images were acquired with a 40x objective in the ApoTome mode. For myotube alignment and orientation, fluorescent and bright-field images were acquired with a 5x objective, and 3 non-overlapping images were acquired for each sample. The groove direction on each PDMS substrate was determined via a bright-field image acquired with a 40x objective (for 500-nm and 800-nm wide grooves) or a 20x objective (for 1000-nm, 1500-nm, and 3000-nm wide grooves). Fluorescent images of HUVECs and 3T3 fibroblasts stained with 2 μM calcein-AM (live cell tracker from Invitrogen) were acquired with a 5x objective.

Fluorescent images of focal adhesions were acquired with a 60x oil objective on an Olympus IX81ZDC inverted spinning disk confocal microscope. Grooves were imaged in bright field.

### 4.5. Analysis of myotube alignment and orientation.

To analyze myotube alignment and orientation, an image acquired with a 5× objective was converted into a binary image using the Otsu auto local threshold command with a radius of 15 pixels, and the binary image was analyzed with Fast Fourier Transformation using the Directionality plugin in ImageJ/Fiji. The output of the Directionality analysis was imported to MatLab and subjected to further processing to yield the probability density function (p.d.f.). Since the Directionality plugin uses the horizontal direction as the 0° reference and reports orientation angles in the range between −90° and 90°, the p.d.f. was adjusted so that the orientation angle is defined as 90° when a myotube aligns perpendicular to grooves and as 0°/180° when a myotube aligns parallel to grooves. The p.d.f. of myotube orientations between 0° and 180° is reported, with the position of the major peak adjusted to fall in the range between 0° and 90° (if the peak falls between 90° and 180°, each angle is converted to 180° minus the angle). If the p.d.f. has a single peak, it was fitted to a Gaussian function (equation (1)) using maximum likelihood estimates in Matlab:

$$f(\theta|\theta_0,\sigma^2)=\frac{1}{\sqrt{2\pi\sigma^2}}e^{-\frac{(\theta-\theta_0)^2}{2\sigma^2}} \quad (1)$$

where $f(\theta)$ is the p.d.f., $\theta_0$ is the mean value, and $\sigma$ is the standard derivation. Each experiment was triplicated and 3 non-overlapping images were acquired for each sample, so 9 images were analyzed for each condition. The revealed mean myotube orientation angles are reported in box- and-whisker plots.

### 4.6. Analysis of focal adhesion distribution on nanogrooved substrates.

Fluorescent intensity distribution profile of paxillin along the muscle alignment direction was calculated by the Plot Profile command in ImageJ/Fiji. The nanogroove spacing profile of the same region was calculated by the same command. The numeric outputs were linearly normalized by setting the lowest intensity value as 0 and the highest intensity value as 100.

### 4.7. Statistical analysis.

Statistical analysis was conducted using one-way analysis of variance (ANOVA) followed by Tukey's post-hoc test.

## Supplementary Material

Refer to Web version on PubMed Central for supplementary material.

## Acknowledgements

This work was supported by the National Science Foundation (CAREER DMR-1151529 for W.S.), by the National Institutes of Arthritis and Musculoskeletal and Skin Diseases of the National Institutes of Health (R01 AR055299 for R.C.R.P.), by the Minnesota Partnership for Biotechnology and Medical Genomics (for Y.A. and S.J.K.), and by Institute for Engineering in Medicine at the University of Minnesota. Portions of this work were carried out in the Minnesota Nano Center, which receives partial support from NSF through the National Nanotechnology Coordinated Infrastructure (NNCI), and the Characterization Facility at the University of Minnesota, which has received capital equipment funding from NSF through the MRSEC program under Award No. DMR-1420013. The cytogenetic analyses were performed in the Cytogenomics Shared Resource at the University of Minnesota with support from the comprehensive Masonic Cancer Center NIH Grant #P30 CA077598-09. We thank James Kiley for assistance with generation of hPSC-derived myogenic progenitors, Yi Ren for assistance with cell sorting, Tony Whipple for assistance with nanofabrication, and Patrick Alford for the use of the confocal microscope. We thank Allison Siehr for proofreading the manuscript.

## References

[1]. Kieny P, Chollet S, Delalande P, Le Fort M, Magot A, Pereon Y, Perrouin Verbe B, Evolution of life expectancy of patients with Duchenne muscular dystrophy at AFM Yolaine de Kepper centre between 1981 and 2011, Ann Phys Rehabil Med 56(6) (2013) 443–54. [PubMed: 23876223]

[2]. Emery AE, Population frequencies of inherited neuromuscular diseases--a world survey, Neuromuscul Disord 1(1) (1991) 19–29. [PubMed: 1822774]

[3]. Blake DJ, Weir A, Newey SE, Davies KE, Function and genetics of dystrophin and dystrophin-related proteins in muscle., Physiol Rev 82(2) (2002) 291–329. [PubMed: 11917091]

[4]. Guiraud S, Aartsma-Rus A, Vieira NM, Davies KE, van Ommen G-JB, Kunkel LM,The Pathogenesis and Therapy of Muscular Dystrophies., Annu Rev Genomics Hum Genet 16 (2015) 281–308. [PubMed: 26048046]

[5]. Ervasti JM, Campbell KP, A Role for the Dystrophin-Glycoprotein Complex as a Transmembrane Linker between Laminin and Actin, Journal of Cell Biology 122(4) (1993) 809–823. [PubMed: 8349731]

[6]. Sanes JR, The basement membrane/basal lamina of skeletal muscle, J Biol Chem 278(15) (2003) 12601–4. [PubMed: 12556454]

[7]. Han R, Kanagawa M, Yoshida-Moriguchi T, Rader EP, Ng RA, Michele DE, Muirhead DE, Kunz S, Moore SA, Iannaccone ST, Miyake K, McNeil PL, Mayer U, Oldstone MB, Faulkner JA, Campbell KP, Basal lamina strengthens cell membrane integrity via the laminin G domain-binding motif of alpha-dystroglycan, Proc Natl Acad Sci U S A 106(31) (2009) 12573–9. [PubMed: 19633189]

[8]. Ervasti JM, Dystrophin, its interactions with other proteins, and implications for muscular dystrophy, Biochim Biophys Acta 1772(2) (2007) 108–17. [PubMed: 16829057]

[9]. Clark KA, McElhinny AS, Beckerle MC, Gregorio CC, Striated muscle cytoarchitecture: an intricate web of form and function, Annu Rev Cell Dev Biol 18 (2002) 637–706. [PubMed: 12142273]

[10]. Petrof BJ, Shrager JB, Stedman HH, Kelly AM, Sweeney HL, Dystrophin protects the sarcolemma from stresses developed during muscle contraction, Proc Natl Acad Sci U S A 90(8) (1993) 3710–4. [PubMed: 8475120]

[11]. Rodino-Klapac LR, Mendell JR, Sahenk Z, Update on the treatment of Duchenne muscular dystrophy., Curr Neurol Neurosci Rep 13(3) (2013) 332. [PubMed: 23328943]

[12]. Ciafaloni E, Fox DJ, Pandya S, Westfield CP, Puzhankara S, Romitti PA, Mathews KD, Miller TM, Matthews DJ, Miller LA, Cunniff C, Druschel CM, Moxley RT, Delayed diagnosis in duchenne muscular dystrophy: data from the Muscular Dystrophy Surveillance, Tracking, and Research Network (MD STARnet), J Pediatr 155(3) (2009) 380–5. [PubMed: 19394035]

[13]. Scully MA, Farrell PM, Ciafaloni E, Griggs RC, Kwon JM, Cystic fibrosis newborn screening: a model for neuromuscular disease screening?, Ann Neurol 77(2) (2015) 189–97. [PubMed: 25425541]

[14]. Falzarano MS, Scotton C, Passarelli C, Ferlini A, Duchenne Muscular Dystrophy: From Diagnosis to Therapy., Molecules 20(10) (2015) 18168–84. [PubMed: 26457695]

[15]. Theadom A, Rodrigues M, Roxburgh R, Balalla S, Higgins C, Bhattacharjee R, Jones K, Krishnamurthi R, Feigin V, Prevalence of muscular dystrophies: a systematic literature review., Neuroepidemiology 43(3–4) (2014) 259–68. [PubMed: 25532075]

[16]. Merlini L, Gennari M, Malaspina E, Cecconi I, Armaroli A, Gnudi S, Talim B, Ferlini A, Cicognani A, Franzoni E, Early corticosteroid treatment in 4 Duchenne muscular dystrophy patients: 14-year follow-up, Muscle Nerve 45(6) (2012) 796–802. [PubMed: 22581531]

[17]. Smith AS, Macadangdang J, Leung W, Laflamme MA, Kim DH, Human iPSC-derived cardiomyocytes and tissue engineering strategies for disease modeling and drug screening, Biotechnol Adv 35(1) (2017) 77–94. [PubMed: 28007615]

[18]. Avior Y, Sagi I, Benvenisty N, Pluripotent stem cells in disease modelling and drug discovery., Nat Rev Mol Cell Biol 17(3) (2016) 170–82. [PubMed: 26818440]

[19]. Liang P, Lan F, Lee AS, Gong T, Sanchez-Freire V, Wang Y, Diecke S, Sallam K, Knowles JW, Wang PJ, Nguyen PK, Bers DM, Robbins RC, Wu JC, Drug screening using a library of human induced pluripotent stem cell-derived cardiomyocytes reveals disease- specific patterns of cardiotoxicity, Circulation 127(16) (2013) 1677–91. [PubMed: 23519760]

[20]. Pa§ca SP, Portmann T, Voineagu I, Yazawa M, Shcheglovitov A, Pa§ca AM, Cord B, Palmer TD, Chikahisa S, Nishino S, Bernstein JA, Hallmayer J, Geschwind DH, Dolmetsch RE, Using iPSC-derived neurons to uncover cellular phenotypes associated with Timothy syndrome, Nat Med 17(12) (2011) 1657–62. [PubMed: 22120178]

[21]. Miller JD, Ganat YM, Kishinevsky S, Bowman RL, Liu B, Tu EY, Mandal PK, Vera E, Shim J.-w., Kriks S, Taldone T, Fusaki N, Tomishima MJ, Krainc D, Milner TA, Rossi DJ, Studer L,

Human iPSC-based modeling of late-onset disease via progerin-induced aging, Cell Stem Cell 13(6) (2013) 691–705. [PubMed: 24315443]

[22]. Passier R, Orlova V, Mummery C, Complex Tissue and Disease Modeling using hiPSCs, Cell Stem Cell 18(3) (2016) 309–21. [PubMed: 26942851]

[23]. Ye L, Chang JC, Lin C, Sun X, Yu J, Kan YW, Induced pluripotent stem cells offer new approach to therapy in thalassemia and sickle cell anemia and option in prenatal diagnosis in genetic diseases, Proceedings of the National Academy of Sciences 106(24) (2009) 9826–9830.

[24]. Darabi R, Arpke RW, Irion S, Dimos JT, Grskovic M, Kyba M, Perlingeiro RCR, Human ES- and iPS-derived myogenic progenitors restore DYSTROPHIN and improve contractility upon transplantation in dystrophic mice., Cell Stem Cell 10(5) (2012) 610–9. [PubMed: 22560081]

[25]. Lee J, Abdeen AA, Zhang D, Kilian KA, Directing stem cell fate on hydrogel substrates by controlling cell geometry, matrix mechanics and adhesion ligand composition, Biomaterials 34(33) (2013) 8140–8. [PubMed: 23932245]

[26]. Lutolf MP, Gilbert PM, Blau HM, Designing materials to direct stem-cell fate, Nature 462(7272) (2009) 433–41. [PubMed: 19940913]

[27]. Dalby MJ, Gadegaard N, Oreffo RO, Harnessing nanotopography and integrin-matrix interactions to influence stem cell fate, Nat Mater 13(6) (2014) 558–69. [PubMed: 24845995]

[28]. Kim D-H, Provenzano PP, Smith CL, Levchenko A, Matrix nanotopography as a regulator of cell function, J Cell Biol 197(3) (2012) 351–60. [PubMed: 22547406]

[29]. Bettinger CJ, Langer R, Borenstein JT, Engineering substrate topography at the micro- and nanoscale to control cell function, Angew Chem Int Ed Engl 48(30) (2009) 5406–15. [PubMed: 19492373]

[30]. Miyoshi H, Adachi T, Topography design concept of a tissue engineering scaffold for controlling cell function and fate through actin cytoskeletal modulation, Tissue Eng Part B Rev 20(6) (2014) 609–27. [PubMed: 24720435]

[31]. Ostrovidov S, Hosseini V, Ahadian S, Fujie T, Parthiban SP, Ramalingam M, Bae H, Kaji H, Khademhosseini A, Skeletal muscle tissue engineering: methods to form skeletal myotubes and their applications, Tissue Eng Part B Rev 20(5) (2014) 403–36. [PubMed: 24320971]

[32]. Smith AST, Davis J, Lee G, Mack DL, Kim DH, Muscular dystrophy in a dish: engineered human skeletal muscle mimetics for disease modeling and drug discovery, Drug Discov Today 21(9) (2016) 1387–1398. [PubMed: 27109386]

[33]. Lam MT, Sim S, Zhu X, Takayama S, The effect of continuous wavy micropatterns on silicone substrates on the alignment of skeletal muscle myoblasts and myotubes, Biomaterials 27(24) (2006) 4340–7. [PubMed: 16650470]

[34]. Ricotti L, Polini A, Genchi GG, Ciofani G, Iandolo D, Vazao H, Mattoli V, Ferreira L, Menciassi A, Pisignano D, Proliferation and skeletal myotube formation capability of C2C12 and H9c2 cells on isotropic and anisotropic electrospun nanofibrous PHB scaffolds, Biomed Mater 7(3) (2012) 035010. [PubMed: 22477772]

[35]. Shimizu K, Fujita H, Nagamori E, Alignment of skeletal muscle myoblasts and myotubes using linear micropatterned surfaces ground with abrasives, Biotechnol Bioeng 103(3) (2009) 631–8. [PubMed: 19189396]

[36]. Yang HS, Ieronimakis N, Tsui JH, Kim HN, Suh K-Y, Reyes M, Kim D-H, Nanopatterned muscle cell patches for enhanced myogenesis and dystrophin expression in a mouse model of muscular dystrophy, Biomaterials 35(5) (2014) 1478–86. [PubMed: 24290810]

[37]. Yang HS, Lee B, Tsui JH, Macadangdang J, Jang SY, Im SG, Kim DH, Electroconductive Nanopatterned Substrates for Enhanced Myogenic Differentiation and Maturation, Adv Healthc Mater 5(1) (2016) 137–45. [PubMed: 25988569]

[38]. Jiao A, Moerk CT, Penland N, Perla M, Kim J, Smith AST, Murry CE, Kim DH, Regulation of skeletal myotube formation and alignment by nanotopographically controlled cell- secreted extracellular matrix, J Biomed Mater Res A 106(6) (2018) 1543–1551. [PubMed: 29368451]

[39]. Jiao A, Trosper NE, Yang HS, Kim J, Tsui JH, Frankel SD, Murry CE, Kim DH, Thermoresponsive nanofabricated substratum for the engineering of three-dimensional tissues with layer-by-layer architectural control, ACS Nano 8(5) (2014) 4430–9. [PubMed: 24628277]

[40]. Tsui JH, Janebodin K, Ieronimakis N, Yama DMP, Yang HS, Chavanachat R, Hays AL, Lee H, Reyes M, Kim DH, Harnessing Sphingosine-1-Phosphate Signaling and Nanotopographical Cues To Regulate Skeletal Muscle Maturation and Vascularization, ACS Nano 11(12) (2017) 11954–11968. [PubMed: 29156133]

[41]. Bettadapur A, Suh GC, Geisse NA, Wang ER, Hua C, Huber HA, Viscio AA, Kim JY, Strickland JB, McCain ML, Prolonged Culture of Aligned Skeletal Myotubes on Micromolded Gelatin Hydrogels, Sci Rep 6 (2016) 28855. [PubMed: 27350122]

[42]. Sengupta D, Gilbert PM, Johnson KJ, Blau HM, Heilshorn SC, Protein-engineered biomaterials to generate human skeletal muscle mimics, Adv Healthc Mater 1(6) (2012) 785–9. [PubMed: 23184832]

[43]. Zhao Y, Zeng H, Nam J, Agarwal S, Fabrication of skeletal muscle constructs by topographic activation of cell alignment, Biotechnol Bioeng 102(2) (2009) 624–31. [PubMed: 18958861]

[44]. Anene-Nzelu CG, Choudhury D, Li H, Fraiszudeen A, Peh KY, Toh YC, Ng SH, Leo HL, Yu H, Scalable cell alignment on optical media substrates, Biomaterials 34(21) (2013) 5078–87. [PubMed: 23601659]

[45]. Hwang Y, Seo T, Hariri S, Choi C, Varghese S, Matrix Topographical Cue-Mediated Myogenic Differentiation of Human Embryonic Stem Cell Derivatives, Polymers 9(11) (2017) 580.

[46]. Ku SH, Park CB, Combined effect of mussel-inspired surface modification and topographical cues on the behavior of skeletal myoblasts, Adv Healthc Mater 2(11) (2013) 1445–50. [PubMed: 23584891]

[47]. Shah R, Knowles JC, Hunt NP, Lewis MP, Development of a novel smart scaffold for human skeletal muscle regeneration, J Tissue Eng Regen Med 10(2) (2016) 162–71. [PubMed: 23878056]

[48]. Huber A, Pickett A, Shakesheff KM, Reconstruction of spatially orientated myotubes in vitro using electrospun, parallel microfibre arrays, European Cells and Materials 14 (2007) 56–63. [PubMed: 17922410]

[49]. Neumann T, Hauschka SD, Sanders JE, Tissue engineering of skeletal muscle using polymer fiber arrays, Tissue Eng 9(5) (2003) 995–1003. [PubMed: 14633383]

[50]. Macadangdang J, Guan X, Smith AST, Lucero R, Czerniecki S, Childers MK, Mack DL, Kim D-H, Nanopatterned Human iPSC-based Model of a Dystrophin-Null Cardiomyopathic Phenotype., Cell Mol Bioeng 8(3) (2015) 320–332. [PubMed: 26366230]

[51]. Kleinman HK, Martin GR, Matrigel: basement membrane matrix with biological activity, Semin Cancer Biol 15(5) (2005) 378–86. [PubMed: 15975825]

[52]. Schindelin J, Arganda-Carreras I, Frise E, Kaynig V, Longair M, Pietzsch T, Preibisch S, Rueden C, Saalfeld S, Schmid B, Tinevez JY, White DJ, Hartenstein V, Eliceiri K, Tomancak P, Cardona A, Fiji: an open-source platform for biological-image analysis, Nat Methods 9(7) (2012) 676–82. [PubMed: 22743772]

[53]. Liu ZQ, Scale space approach to directional analysis of images, Appl Opt 30(11) (1991) 1369–73. [PubMed: 20700292]

[54]. Junkin M, Leung SL, Whitman S, Gregorio CC, Wong PK, Cellular self-organization by autocatalytic alignment feedback, J Cell Sci 124(Pt 24) (2011) 4213–20. [PubMed: 22193956]

[55]. Hohenester E, Yurchenco PD, Laminins in basement membrane assembly, Cell Adh Migr 7(1) (2013) 56–63. [PubMed: 23076216]

[56]. Hohenester E, Tisi D, Talts JF, Timpl R, The Crystal Structure of a Laminin G--like Module Reveals the Molecular Basis of α-Dystroglycan Binding to Laminins, Perlecan, and Agrin, Molecular cell 4(5) (1999) 783–792. [PubMed: 10619025]

[57]. Darabi R, Gehlbach K, Bachoo RM, Kamath S, Osawa M, Kamm KE, Kyba M, Perlingeiro RCR, Functional skeletal muscle regeneration from differentiating embryonic stem cells, Nat Med 14(2) (2008) 134–43. [PubMed: 18204461]

[58]. Yaffe D, Saxel O, Serial passaging and differentiation of myogenic cells isolated from dystrophic mouse muscle, Nature 270(5639) (1977) 725–7. [PubMed: 563524]

[59]. Mohammadi MH, Obregon R, Ahadian S, Ramon-Azcon J, Radisic M, Engineered Muscle Tissues for Disease Modeling and Drug Screening Applications, Curr Pharm Des 23(20) (2017) 2991–3004. [PubMed: 28215153]

[60]. Carson D, Hnilova M, Yang X, Nemeth CL, Tsui JH, Smith AS, Jiao A, Regnier M, Murry CE, Tamerler C, Kim DH, Nanotopography-Induced Structural Anisotropy and Sarcomere Development in Human Cardiomyocytes Derived from Induced Pluripotent Stem Cells, ACS Appl Mater Interfaces 8(34) (2016) 21923–32. [PubMed: 26866596]

[61]. Abadi PPSS, Garbern JC, Behzadi S, Hill MJ, Tresback JS, Heydari T, Ejtehadi MR, Ahmed N, Copley E, Aghaverdi H, Lee RT, Farokhzad OC, Mahmoudi M, Engineering of Mature Human Induced Pluripotent Stem Cell-Derived Cardiomyocytes Using Substrates with Multiscale Topography, Advanced Functional Materials 28(19) (2018) 1707378.

[62]. Luna JI, Ciriza J, Garcia-Ojeda ME, Kong M, Herren A, Lieu DK, Li RA, Fowlkes CC, Khine M, McCloskey KE, Multiscale biomimetic topography for the alignment of neonatal and embryonic stem cell-derived heart cells, Tissue Eng Part C Methods 17(5) (2011) 579–88. [PubMed: 21235325]

[63]. Wang J, Chen A, Lieu DK, Karakikes I, Chen G, Keung W, Chan CW, Hajjar RJ, Costa KD, Khine M, Li RA, Effect of engineered anisotropy on the susceptibility of human pluripotent stem cell-derived ventricular cardiomyocytes to arrhythmias, Biomaterials 34(35) (2013) 8878–86. [PubMed: 23942210]

[64]. Shum AM, Che H, Wong AO, Zhang C, Wu H, Chan CW, Costa K, Khine M, Kong CW, Li RA, A Micropatterned Human Pluripotent Stem Cell-Based Ventricular Cardiac Anisotropic Sheet for Visualizing Drug-Induced Arrhythmogenicity, Adv Mater 29(1) (2017).

[65]. Rao C, Prodromakis T, Kolker L, Chaudhry UA, Trantidou T, Sridhar A, Weekes C, Camelliti P, Harding SE, Darzi A, Yacoub MH, Athanasiou T, Terracciano CM, The effect of microgrooved culture substrates on calcium cycling of cardiac myocytes derived from human induced pluripotent stem cells, Biomaterials 34(10) (2013) 2399–411. [PubMed: 23261219]

[66]. Gouveia PJ, Rosa S, Ricotti L, Abecasis B, Almeida HV, Monteiro L, Nunes J, Carvalho FS, Serra M, Luchkin S, Kholkin AL, Alves PM, Oliveira PJ, Carvalho R, Menciassi A, das Neves RP, Ferreira LS, Flexible nanofilms coated with aligned piezoelectric microfibers preserve the contractility of cardiomyocytes, Biomaterials 139 (2017) 213–228. [PubMed: 28622605]

[67]. Pall EA, Bolton KM, Ervasti JM, Differential heparin inhibition of skeletal muscle alpha-dystroglycan binding to laminins, J Biol Chem 271(7) (1996) 3817–21. [PubMed: 8631999]

[68]. Brown SC, Fassati A, Popplewell L, Page AM, Henry MD, Campbell KP, Dickson G, Dystrophic phenotype induced in vitro by antibody blockade of muscle alpha-dystroglycan- laminin interaction, Journal of cell science 112(2) (1999) 209–216. [PubMed: 9858474]

[69]. Tsang KM, Annabi N, Ercole F, Zhou K, Karst D, Li F, Haynes JM, Evans RA, Thissen H, Khademhosseini A, Forsythe JS, Facile One-step Micropatterning Using Photodegradable Methacrylated Gelatin Hydrogels for Improved Cardiomyocyte Organization and Alignment, Adv Funct Mater 25(6) (2015) 977–986. [PubMed: 26327819]

[70]. Teixeira AI, McKie GA, Foley JD, Bertics PJ, Nealey PF, Murphy CJ, The effect of environmental factors on the response of human corneal epithelial cells to nanoscale substrate topography, Biomaterials 27(21) (2006) 3945–54. [PubMed: 16580065]

[71]. Rajnicek A, Britland S, McCaig C, Contact guidance of CNS neurites on grooved quartz: influence of groove dimensions, neuronal age and cell type, J Cell Sci 110 ( Pt 23) (1997) 2905–13. [PubMed: 9359873]

[72]. Nagata I, Nakatsuji N, Rodent CNS neuroblasts exhibit both perpendicular and parallel contact guidance on the aligned parallel neurite bundle, Development 112(2) (1991) 581–90. [PubMed: 1794326]

[73]. Evans DJ, Britland S, Wigmore PM, Differential response of fetal and neonatal myoblasts to topographical guidance cues in vitro, Dev Genes Evol 209(7) (1999) 438–42. [PubMed: 10370128]

[74]. Guex AG, Birrer DL, Fortunato G, Tevaearai HT, Giraud MN, Anisotropically oriented electrospun matrices with an imprinted periodic micropattern: a new scaffold for engineered muscle constructs, Biomed Mater 8(2) (2013) 021001. [PubMed: 23343525]

[75]. Tamiello C, Buskermolen ABC, Baaijens FPT, Broers JLV, Bouten CVC, Heading in the Right Direction: Understanding Cellular Orientation Responses to Complex Biophysical Environments, Cell Mol Bioeng 9 (2016) 12–37. [PubMed: 26900408]

[76]. Uttayarat P, Toworfe GK, Dietrich F, Lelkes PI, Composto RJ, Topographic guidance of endothelial cells on silicone surfaces with micro- to nanogrooves: orientation of actin filaments and focal adhesions, J Biomed Mater Res A 75(3) (2005) 668–80. [PubMed: 16110489]

[77]. Parsons JT, Horwitz AR, Schwartz MA, Cell adhesion: integrating cytoskeletal dynamics and cellular tension, Nat Rev Mol Cell Biol 11(9) (2010) 633–43. [PubMed: 20729930]

[78]. Yim EKF, Darling EM, Kulangara K, Guilak F, Leong KW, Nanotopography-induced changes in focal adhesions, cytoskeletal organization, and mechanical properties of human mesenchymal stem cells, Biomaterials 31(6) (2010) 1299–306. [PubMed: 19879643]

[79]. Butt T, Mufti T, Humayun A, Rosenthal PB, Khan S, Khan S, Molloy JE, Myosin motors drive long range alignment of actin filaments, J Biol Chem 285(7) (2010) 4964–74. [PubMed: 19940124]

[80]. Sparrow JC, Schock F, The initial steps of myofibril assembly: integrins pave the way, Nat Rev Mol Cell Biol 10(4) (2009) 293–8. [PubMed: 19190670]

[81]. Quach NL, Rando TA, Focal adhesion kinase is essential for costamerogenesis in cultured skeletal muscle cells, Dev Biol 293(1) (2006) 38–52. [PubMed: 16533505]

[82]. Raeker MO, Shavit JA, Dowling JJ, Michele DE, Russell MW, Membrane-myofibril cross-talk in myofibrillogenesis and in muscular dystrophy pathogenesis: lessons from the zebrafish, Front Physiol 5 (2014) 14. [PubMed: 24478725]

[83]. Hidalgo M, Sirour C, Bello V, Moreau N, Beaudry M, Darribere T, In vivo analyzes of dystroglycan function during somitogenesis in Xenopus laevis, Dev Dyn 238(6) (2009) 1332–45. [PubMed: 19086027]

[84]. Perez-Moreno JJ, Bischoff M, Martin-Bermudo MD, Estrada B, The conserved transmembrane proteoglycan Perdido/Kon-tiki is essential for myofibrillogenesis and sarcomeric structure in Drosophila, J Cell Sci 127(Pt 14) (2014) 3162–73. [PubMed: 24794494]

[85]. Teixeira AI, Abrams GA, Bertics PJ, Murphy CJ, Nealey PF, Epithelial contact guidance on well-defined micro- and nanostructured substrates, J Cell Sci 116(Pt 10) (2003) 1881–92. [PubMed: 12692189]

[86]. Biggs MJP, Richards RG, Wilkinson CDW, Dalby MJ, Focal adhesion interactions with topographical structures: a novel method for immuno-SEM labelling of focal adhesions in S-phase cells, Journal of microscopy 231(1) (2008) 28–37. [PubMed: 18638187]

[87]. Lamers E, van Horssen R, te Riet J, van Delft F, Luttge R, Walboomers XF, Jansen JA, The influence of nanoscale topographical cues on initial osteoblast morphology and migration, European Cells and Materials 20 (2010) 329–343. [PubMed: 21061239]

[88]. Gautrot JE, Malmstrom J, Sundh M, Margadant C, Sonnenberg A, Sutherland DS, The nanoscale geometrical maturation of focal adhesions controls stem cell differentiation and mechanotransduction, Nano Lett 14(7) (2014) 3945–52. [PubMed: 24848978]

[89]. Lutz R, Pataky K, Gadhari N, Marelli M, Brugger J, Chiquet M, Nano-stenciled RGD- gold patterns that inhibit focal contact maturation induce lamellipodia formation in fibroblasts, PLoS One 6(9) (2011) e25459. [PubMed: 21980465]

[90]. Iannone M, Ventre M, Formisano L, Casalino L, Patriarca EJ, Netti PA, Nanoengineered surfaces for focal adhesion guidance trigger mesenchymal stem cell self-organization and tenogenesis, Nano Lett 15(3) (2015) 1517–25. [PubMed: 25699511]

[91]. Ervasti JM, Costameres: the Achilles' heel of Herculean muscle, J Biol Chem 278(16) (2003) 13591–4. [PubMed: 12556452]

[92]. Straub V, Campbell KP, Muscular dystrophies and the dystrophin-glycoprotein complex, Curr Opin Neurol 10(2) (1997) 168–75. [PubMed: 9146999]

[93]. Lapidos KA, Kakkar R, McNally EM, The dystrophin glycoprotein complex: signaling strength and integrity for the sarcolemma, Circ Res 94(8) (2004) 1023–31. [PubMed: 15117830]

[94]. Campbell KP, Three muscular dystrophies: loss of cytoskeleton-extracellular matrix linkage, Cell 80(5) (1995) 675–679. [PubMed: 7889563]

[95]. Worton R, Muscular dystrophies: diseases of the dystrophin-glycoprotein complex, Science 270(5237) (1995) 755–6. [PubMed: 7481760]

[96]. Gintjee TJJ, Magh ASH, Bertoni C, High throughput screening in duchenne muscular dystrophy: from drug discovery to functional genomics., Biology (Basel) 3(4) (2014) 752–80. [PubMed: 25405319]

[97]. Moorwood C, Soni N, Patel G, Wilton SD, Khurana TS, A cell-based high-throughput screening assay for posttranscriptional utrophin upregulation., J Biomol Screen 18(4) (2013) 400–6. [PubMed: 23112083]

[98]. Tang S, Xie M, Cao N, Ding S, Patient-Specific Induced Pluripotent Stem Cells for Disease Modeling and Phenotypic Drug Discovery., J Med Chem 59(1) (2016) 2–15. [PubMed: 26322868]

[99]. Anighoro A, Bajorath J, Rastelli G, Polypharmacology: challenges and opportunities in drug discovery, J Med Chem 57(19) (2014) 7874–87. [PubMed: 24946140]

[100]. Endo T, Glycobiology of a-dystroglycan and muscular dystrophy., J Biochem 157(1) (2015) 1–12. [PubMed: 25381372]

[101]. Liu B, Liu Y, Riesberg JJ, Shen W, Dynamic presentation of immobilized ligands regulated through biomolecular recognition, J Am Chem Soc 132(39) (2010) 13630–2. [PubMed: 20839864]

[102]. Magli A, Incitti T, Kiley J, Swanson SA, Darabi R, Rinaldi F, Selvaraj S, Yamamoto A, Tolar J, Yuan C, Stewart R, Thomson JA, Perlingeiro RCR, PAX7 Targets, CD54, Integrin alpha9beta1, and SDC2, Allow Isolation of Human ESC/iPSC-Derived Myogenic Progenitors, Cell Rep 19(13) (2017) 2867–2877. [PubMed: 28658631]

## Highlight Points

➢Non-diseased myotubes align perpendicular to nanogrooves on substrates having laminin.

➢Nanogrooved, laminin-modified substrates distinguish non-diseased and DMD myotubes.

➢This phenotypic biomarker may facilitate DMD drug development and early diagnosis.

➢All myotubes align parallel to grooves when grooves are larger or laminin is missing.

➢The DAPC and its interaction with laminin regulate perpendicular myotube alignment.

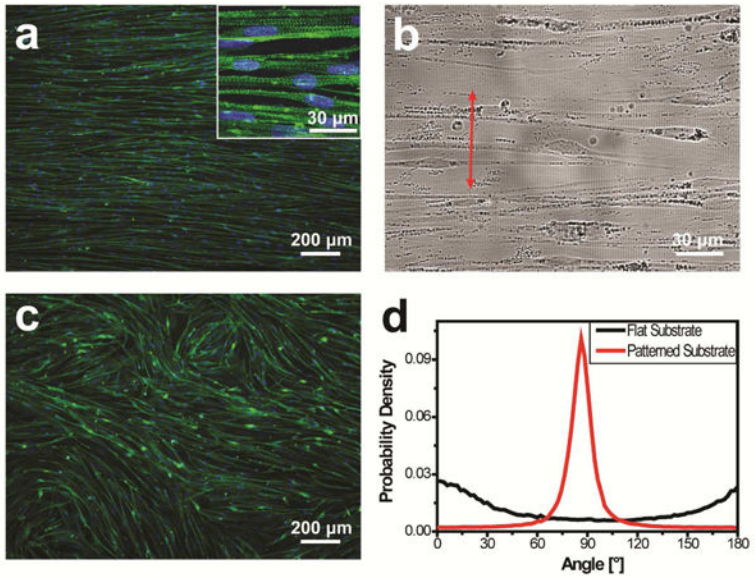


**Figure 1.**

Alignment and orientation of myotubes differentiated from hESC-derived myogenic progenitors on Matrigel-functionalized substrates patterned with 800-nm wide topographical grooves. (a) Cells differentiated into myotubes possessing sarcomeres (inset) and aligned in a consistent direction throughout the entire substrate. Cells were immunofluorescently stained for sarcomeric a-actinin (green) and nuclei were counter-stained with Hoechst 33342 (blue). (b) The nanogrooove direction (arrowed red line) was determined via bright-field imaging, revealing nearly perpendicular orientation of the aligned myotubes relative to nanogrooves. (c) Myotubes cultured on flat control substrates oriented randomly. (d) The p.d.f of myotube orientations has a single, narrow, and high peak near 90° for cells cultured on the nanogrooved substrates, but not for cells cultured on flat control substrates. The cells were cultured for 2 weeks after differentiation induction.

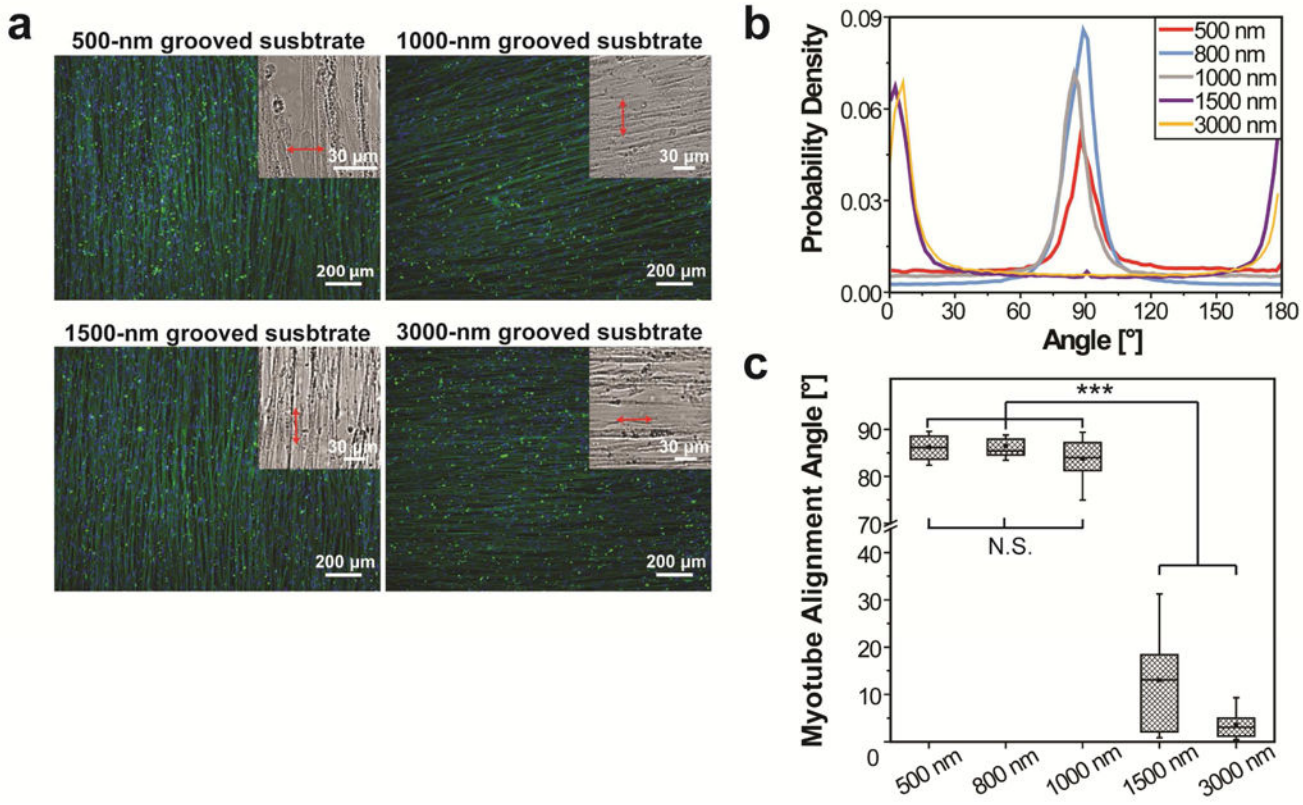


**Figure 2.**

The effects of the groove feature size on alignment and orientation of myotubes differentiated from hESC-derived myogenic progenitors on Matrigel-functionalized substrates. (a) Myotubes aligned in a consistent direction throughout each entire substrate, but their orientation relative to the groove direction varied with the groove feature size. Myotubes aligned nearly perpendicular to 500-nm and 1000-nm wide grooves (as those on 800-nm grooved substrates shown in Figure 1), but aligned nearly parallel to 1500-nm and 3000-nm wide grooves. Cells were immunofluorescently stained for sarcomeric α-actinin (green) and nuclei were counter-stained with Hoechst 33342 (blue). Insets: bright-field images used to determine the groove directions (arrowed red lines). (b) The p.d.f. of myotube orientations has a single, narrow, and high peak near 90° when the groove feature size is 500 nm, 800 nm, and 1000 nm and has a peak near 0°/180° when the groove feature size is 1500 nm and 3000 nm. (c) The p.d.f. curves were fitted to a Gaussian function and the revealed mean myotube orientation angles are shown as box-and-whisker plots: box marks the 25th to 75th percentiles, horizontal line marks the median, whiskers mark the minimum and maximum, dot marks the mean (n=9 for each condition). The cells were cultured for 2 weeks after differentiation induction. (N.S.= no significant difference, ***$p<0.0001$ by one-way ANOVA)

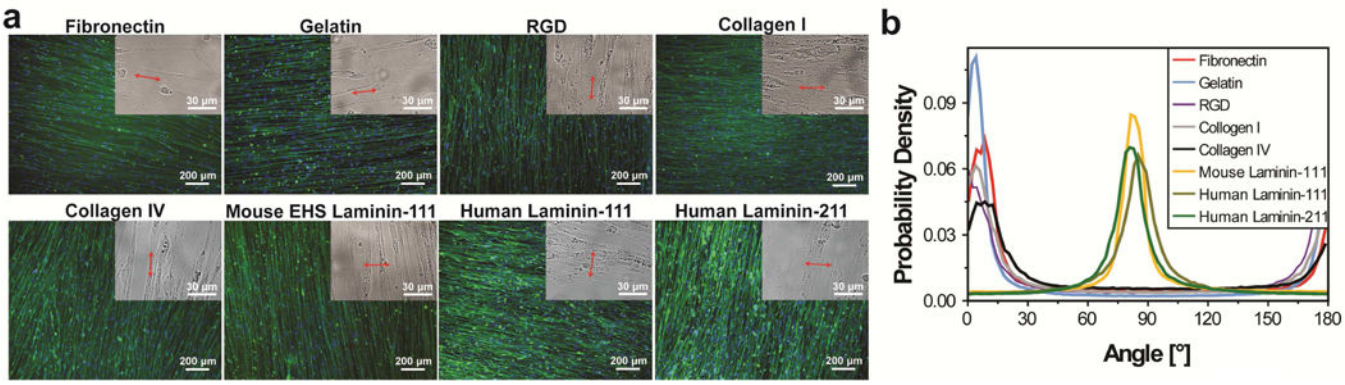


**Figure 3.**

The effects of substrate-bound cell adhesion molecules on alignment and orientation of myotubes differentiated from hESC-derived myogenic progenitors on 800-nm grooved substrates. (a) Myotubes aligned in a consistent direction on each of the substrates functionalized with gelatin, RGD peptide, fibronectin, type I collagen, type IV collagen, and laminin respectively. Aligned myotubes oriented nearly perpendicular to nanogrooves on substrates functionalized with EHS mouse laminin-111, human laminin-111, and human laminin-211, and oriented nearly parallel to nanogrooves on all other substrates. Images are shown as in Figure 2a. (b) The p.d.f. of myotube orientations has a single, narrow, and high peak for all the samples; the peak is near 90° for cells cultured on laminin-functionalized substrates and near 0°/180° for cells cultured on all other substrates. The cells were cultured for 2 weeks after differentiation induction.

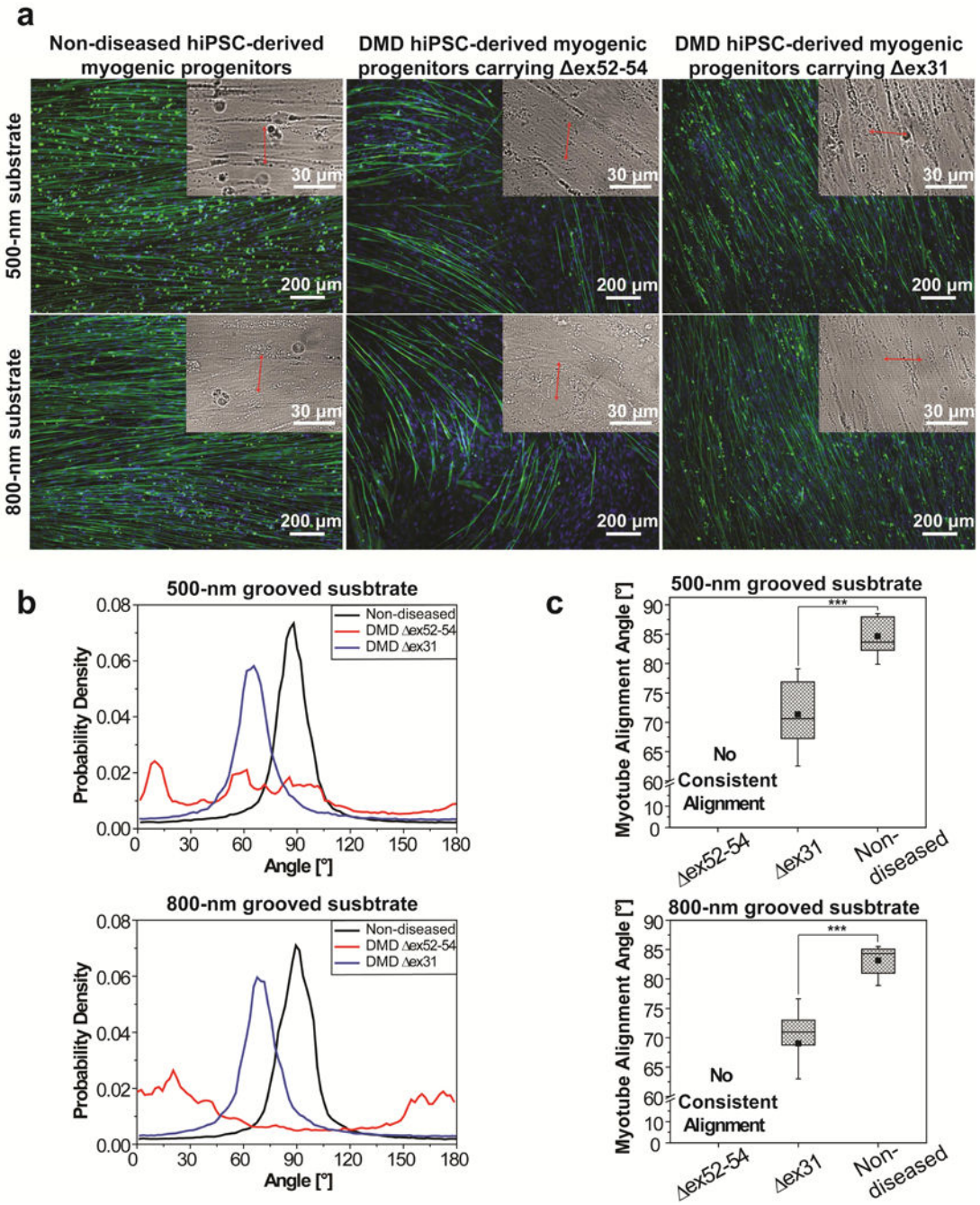


**Figure 4.**

Myotubes differentiated from non-diseased hiPSC-derived myogenic progenitors, primary human skeletal myoblasts, mESC-derived myogenic progenitors, and C2C12 cells could also align nearly perpendicular to nanogrooves on Matrigel-functionalized substrates, suggesting that this phenotype might be universal for muscle cells regardless of their origins and species. Images are shown as in Figure 2a. The cells were cultured for 2 weeks after differentiation induction.

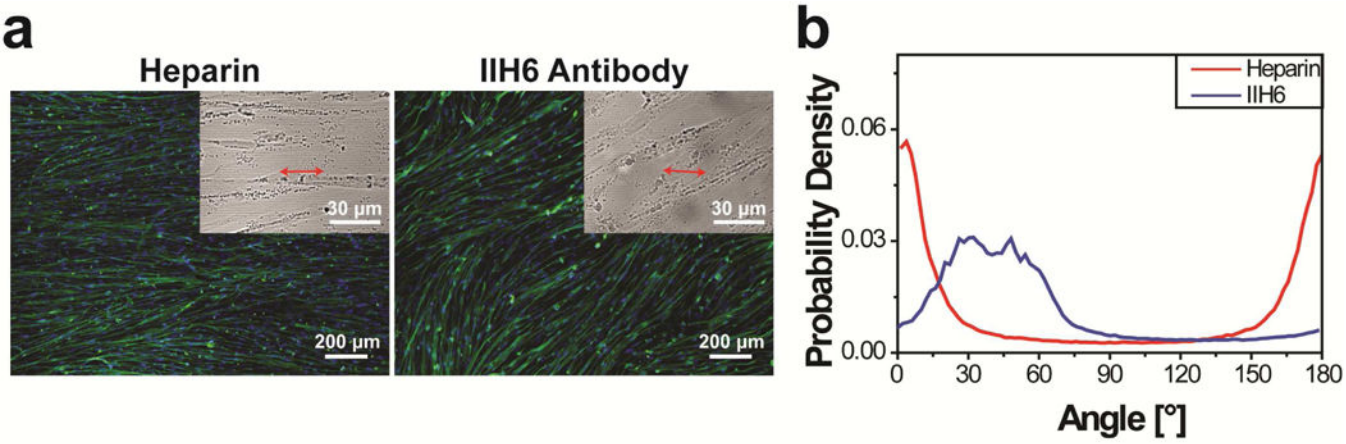


**Figure 5.**

Myotube alignment and orientation on Matrigel-functionalized, nanogrooved substrates allows investigators blinded to the experimental groups to accurately distinguish myogenic progenitors derived from non-diseased hiPSCs, DMD hiPSCs carrying the Δex52–54 mutation that completely nullifies dystrophin, and DMD hiPSCs carrying the Δex31 mutation that allows partially functional dystrophin to be produced, (a) Myotubes differentiated from the three cell types exhibited strikingly different alignment and orientation. Images are shown as in Figure 2a (b) The curves of the p.d.f. of myotube orientations for the three cell types are distinct, (c) The p.d.f. curves having a single peak were fitted to a Gaussian function and the revealed mean myotube orientation angles are shown as box-and-whisker plots (n=9 for each condition). Box- and-whisker plots are shown as in Figure 2c. Cells were cultured for 2 weeks after differentiation induction. (***$p<0.0001$ by one-way ANOVA)

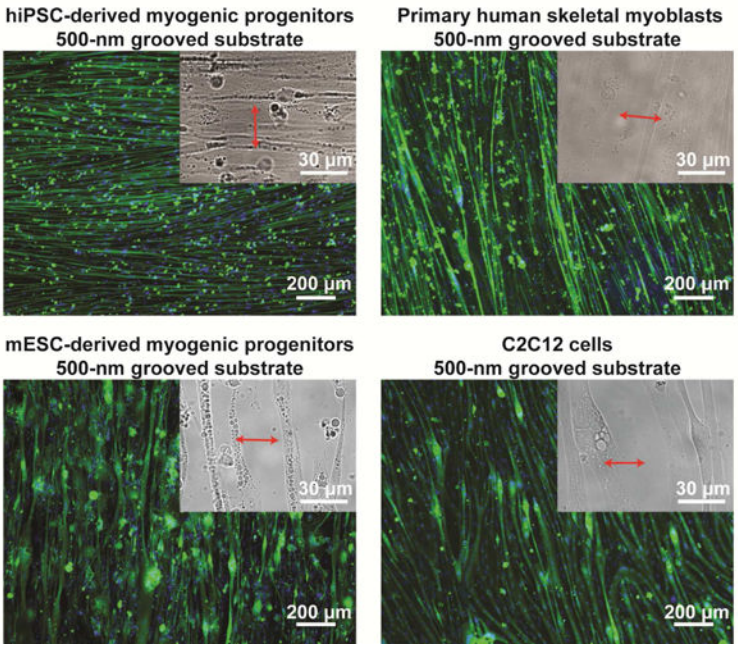


**Figure 6.**

Disruption of the DAPC-laminin interaction disenables hESC-derived myotubes to align perpendicular to nanogrooves on Matrigel-functionalized, 800-nm grooved substrates, (a) In the presence of 1 mg/ml heparin (which binds to laminin) or 70 μg/ml anti-α-dystroglycan antibody IIH6, myotube orientations deviated substantially from the perpendicular direction relative to the nanogrooves. Images are shown as in Figure 2a. (b) The p.d.f. of myotube orientations shows a high peak near 0° for the cells cultured in the presence of heparin and a wide, low peak near 40° for the cells cultured in the presence of IIH6. The cells were cultured for 2 weeks after differentiation induction.

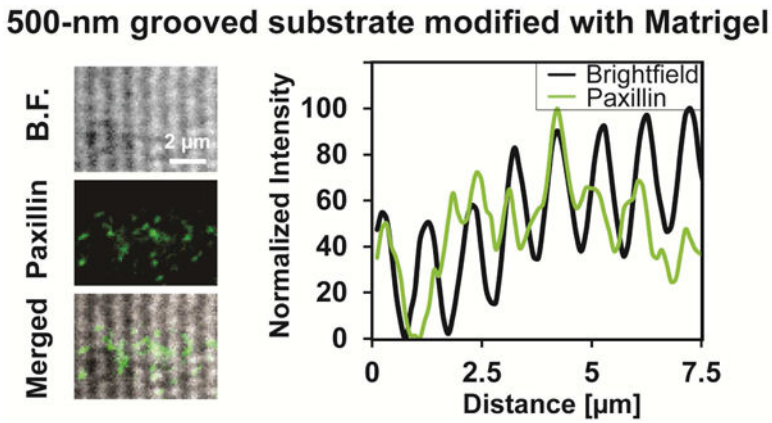


**Figure 7.**

Focal adhesions are mainly constrained on ridges when the feature size is submicron, as shown by the overlay of the bright field (B.F.) image of the pattern and the fluorescent image of paxillin. Images are further analyzed by overlaying the paxillin distribution profile and the nanogroove spacing profile of the same region. Cells were cultured for 3 days after differentiation induction.

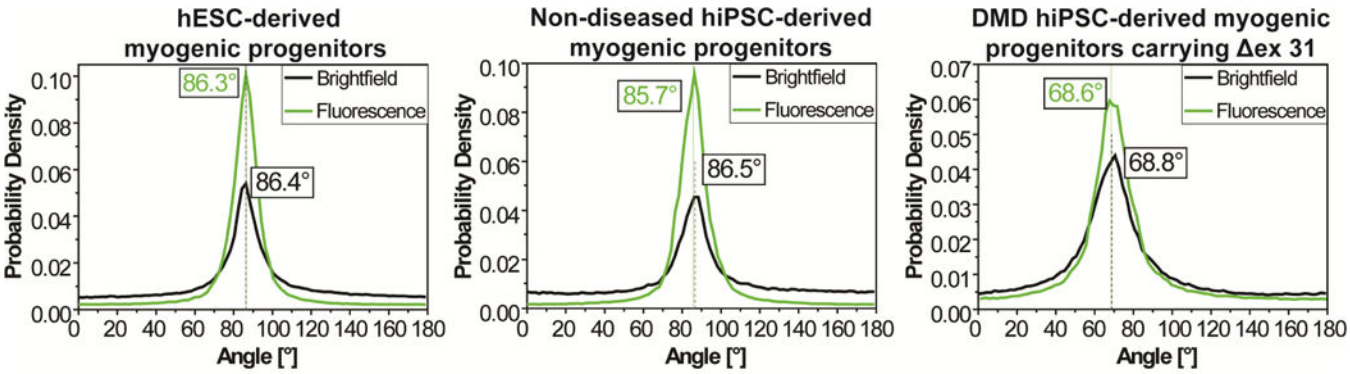


**Figure 8.**

Quantitative analyses of myotube alignment and orientation on the basis of bright-field and fluorescent images of the same frame yield highly consistent results for all tested conditions. All the cells were cultured on Matrigel-functionalized, 800-nm grooved substrates. The dashed line for each p.d.f. curve represents the mean myotube orientation angle from Gaussian curve fitting.